journal

J. Am. Ceram. Soc., 94 [5] 1380–1387 (2011)
DOI: 10.1111/j.1551-2916.2010.04260.x

Effect of SiO_2 on Densification and Microstructure Development in Nd:YAG Transparent Ceramics

Adam J. Stevenson,[†,‡] Xin Li,[‡] Miguel A. Martinez,[‡] Julie M. Anderson,[‡] Daniel L. Suchy,[§] Elizabeth R. Kupp,[‡] Elizabeth C. Dickey,[‡] Karl T. Mueller,[§] and Gary L. Messing[‡]

[‡]Department of Materials Science and Engineering and Materials Research Institute, The Pennsylvania State University, University Park, Pennsylvania 16802

[§]Department of Chemistry, The Pennsylvania State University, University Park, Pennsylvania 16802

This paper examines the influence of SiO_2 doping on densification and microstructure evolution in $Nd_{3x}Y_{3-3x}Al_5O_{12}$ (Nd:YAG) ceramics. Nd:YAG powders were doped with 0.035–0.28 wt% SiO_2 and vacuum sintered between 1484° and 1750°C. ^{29}Si magic-angle spinning nuclear magnetic resonance showed that Si^{4+} substitutes onto tetrahedrally coordinated Al^{3+} sites. High-resolution transmission electron microscopy showed no grain boundary second phases for all silica levels in samples sintered at 1600°–1750°C. Coarsening was limited by a solute drag mechanism as suggested by cubic grain growth kinetics and transmission electron microscopy energy-dispersive X-ray spectroscopy observations of increased Nd^{3+} concentration near grain boundaries. Increasing SiO_2 content increased both densification and grain growth rate and led to increasingly coarsening-dominated sintering trajectories. Fine-grained (<3 μm), highly transparent (>82% real in-line transmission) ceramics were produced by sintering 0.035 wt% SiO_2-doped ceramics at 1750°C for 8 h. Coarse-grained (18 μm), transparent samples were obtained with 0.28 wt% SiO_2-doped Nd:YAG when sintered at 1600°C for 8 h.

I. Introduction

Coble first demonstrated that polycrystalline ceramics could be sintered to a visually translucent/transparent state.[1] Peelan and Metselaar[2] showed that the primary scattering sites in translucent alumina were pores and highly transparent ceramics could only be achieved by eliminating residual porosity. Since then, a variety of transparent materials including Yttralox ($90\%Y_2O_3$–$10\%ThO_2$),[3] $MgAl_2O_4$,[4] and AlON[5] have been successfully produced by sintering to exceptionally high densities (i.e., >99.9%) and thus reducing/eliminating light scattering from residual porosity. In many cases, pressure assisted densification (hot pressing (HP) and/or hot isostatic pressing (HIP)) is used to eliminate the final few pores in transparent ceramics, but contamination and cost concerns inherent to HP and HIP make pressureless sintering the preferred process when possible. While there are many studies about final stage densification and microstructure evolution in ceramics, few studies have concentrated on sintering and microstructure development at the exceptionally high densities required for transparent ceramics (>99.9%). In this paper, we examine these issues for $Nd_{3x}Y_{3-3x}Al_5O_{12}$ (Nd:YAG) ceramics, a material system of current interest for advanced solid-state lasers.

There is substantial interest in transparent Nd:YAG and other ceramic laser hosts (Sc_2O_3, Y_2O_3, $Y_3A_5O_{12}$) doped with optically active ions (Nd^{3+}, Er^{3+}, Yb^{3+}, Tm^{2+}, Ho^{4+}).[6–11] Where direct comparisons are possible, ceramic laser hosts have similar optical properties, lasing threshold, and lasing efficiency as melt-grown single crystals.[6] At high laser powers, Nd:YAG ceramics may show higher total output power than Czochralski grown single crystals because ceramics do not contain certain defects inherent to the Czochralski process.[12,13]

Transparent Nd:YAG ceramics are fabricated by sintering Y_2O_3, Al_2O_3, and Nd_2O_3 powders (solid-state reactionr (SSR)) or solution-derived Nd:YAG powders. Ikesue *et al.*[6] showed that doping an SSR system with 0.14 wt% SiO_2 was critical to achieving transparency and enabled laser slope efficiencies similar to Czochralski grown crystals. All subsequent literature reports about sintering transparent Nd:YAG ceramics (both SSR and YAG powder approaches) use SiO_2 as a sintering aid.

Fine-grained (1–5 μm) ceramic laser host materials are desirable for high power applications because they have higher strength and thus can perform at higher maximum output powers than coarse-grained (>10 μm) ceramics. Finer grain sizes also improve laser performance by mitigating thermally induced optical birefringence effects between grains, thus enabling temporally stable laser output.[14]

Grain sizes between 10 and 50 μm are common to SSR synthesized Nd:YAG as a result of the >1725°C sintering temperature required to achieve full density.[6,10,11] In 2002, Lu *et al.*[15] reported highly transparent, laser quality Nd:YAG by sintering coprecipitated powders. These ceramics (available through Konoshima Chemical Inc., Osaka, Japan) are ≈2 μm grain size and demonstrate lasing efficiency and output power similar to single crystals.[8] Recently, Lee *et al.*[16] demonstrated fine-grained (2–3 μm), transparent Nd:YAG densified by a sinter-HIP process between 1600° and 1750°C. By the HIP approach, Lee and colleagues showed that silica content could be reduced to 0.04 wt% while still producing ceramics with in-line transmission >82% at 1064 nm (the lasing wavelength in Nd:YAG).

Thermodynamic modeling of the SiO_2–Y_2O_3–Al_2O_3 system shows that SiO_2 forms a liquid phase with YAG at temperatures >1400°C.[17] However, SiO_2 solid solution in the YAG lattice was not included in the thermodynamic model.[17] Boulesteix *et al.*[18] used densification kinetics and scanning electron microscopy (SEM) observations to determine that a liquid phase does develop in 0.3 wt% SiO_2-doped YAG ceramics sintered between 1400° and 1550°C. However, high-resolution transmission electron microscopy (HRTEM) images of grain boundaries in transparent YAG and Nd:YAG samples sintered between 1675° and 1750°C and cooled at ≥20°C/min revealed no evidence of an amorphous phase at grain boundaries or triple lines.[16,19]

To understand how SiO_2 interacts with the YAG lattice, first consider the following crystal features. $Y_3Al_5O_{12}$ has a cubic crystal structure (space group *Ia*3*d* or O_h^{10}) with 160 atoms (eight

A. Krell—contributing editor

Manuscript No. 28190. Received June 16, 2010; approved October 17, 2010.
This work was supported by the United States National Science Foundation grant number DMR749391.
[†]Author to whom correspondence should be addressed. e-mail: ajsteven130@gmail.com

formula units) per unit cell and lattice constant = 12.000 Å. Y^{3+} (0.1019 nm) occupies dodecahedrally coordinated 24(*c*) sites. Al^{3+} occupies two crystallographically distinct sites: octahedrally coordinated 16(*a*) sites (0.0535nm) and tetrahedrally coordinated 24(*d*) sites (0.039 nm). O^{2-} occupies the 96(*h*) sites that make up the vertices between the cation polyhedra. Each O^{2-} is shared between two Y^{3+} dodecahedra, one Al^{3+} tetrahedron, and one Al^{3+} octahedron. Nd^{3+} (0.1109 nm) substitutes for Y^{3+} onto the dodecahedrally coordinated 24(*c*) sites resulting in a lattice strain due to its larger ionic radius.

Several defect mechanisms have been proposed for SiO_2 solubility in YAG. Based on atomistic modeling, Kuklja predicted that the most likely defect mechanism for Si^{4+} (0.026 nm) solubility in YAG is

$$SiO_2 + \frac{5}{6}Al_{Al}^{x} + \frac{1}{2}Y_{Y}^{x} \rightarrow Si'_{Al} + \frac{1}{3}V_{Y}'' + \frac{1}{6}Y_3Al_5O_{12} \qquad (1)$$

where the preferred substitutional site is the tetrahedrally coordinated 24(*d*) site.[20] This seems logical due to the similar ionic radii of tetrahedrally coordinated Si^{4+} (0.026 nm) and the 24(*d*) tetrahedral Al^{3+} sites (0.039nm) in YAG.

In this article, we determine the local chemical environment surrounding Si^{4+} in SiO_2-doped Nd:YAG ceramics and discuss how SiO_2 doping affects mass transport mechanisms, densification, and grain growth between 1600° and 1750°C. Further, we demonstrate how sintering trajectory is affected by changing SiO_2 content and how this information can be used to obtain either coarse-grained (>10 μm) or fine-grained (<3 μm) highly transparent Nd:YAG ceramics. We also discuss the influence of green forming on sintering trajectory and the ability to produce fine-grained, highly transparent Nd:YAG ceramics. Coprecipitated Nd:YAG powders are used in this study, however the results are applicable to SSR derived Nd:YAG ceramics as well because phase formation in SSR powders is complete by 1500°C.

II. Experimental Procedure

(1) Powder Synthesis and Green Forming

Nd:YAG powders were synthesized by reverse strike coprecipitation of 1.5*M* aqueous solutions of $Al(NO_3)_3 \cdot 9H_2O$ (98+%, Sigma-Aldrich, St. Louis, MO), YCl_3, and $Nd(NO_3)_3 \cdot nH_2O$ (99.9%, Alfa Aesar, Ward Hill, MA). 1.5*M* YCl_3 was prepared by dissolving Y_2O_3 powder (99.99%, Yarmouth Inc., Danbury, CT) in HCl (J.T. Baker, Phillipsburg, NJ). The salt solution was added dropwise to a rapidly stirring aqueous solution of 0.45*M* $(NH_4)_2SO_4$. The precipitation pH was maintained at 9.2 with NH_4OH. After aging for 1 h, the precipitate was repeatedly washed and centrifuged with 0.05*M* $(NH_4)_2SO_4$ and a final wash was performed using ethanol. The washed precipitate was dried for 16 h at 80°C and crushed in a mortar and pestle. The coprecipitated powder was calcined at 1150°C for 2 h to form the garnet phase and subsequently calcined at 1250°C for 12 h to increase the average particle size to 200 nm (Fig. 1). Each powder particle is composed of two to three 80 nm crystallites. All powders used in this study were 1at.% Nd:YAG, and will be referred to simply as Nd:YAG.

The Nd:YAG powders were mixed with different amounts of tetraethoxysilane (TEOS, 99.9999%, Alfa Aesar) to obtain 0.035, 0.07, 0.14, and 0.28 wt% SiO_2 doped 1 at.% Nd:YAG. The Nd:YAG powder for each composition was taken from a single powder batch, thus the stoichiometry is identical for each composition. Powder batches were ball milled in anhydrous ethanol (reagent grade, J.T. Baker) for 16 h using high purity Al_2O_3 balls (99.9%, 5 mm diameter, Nikkato Corp., Sakai, Japan). The volume ratio of powder:milling media:alcohol was 1:4:8, and the milling media had no measureable weight loss after milling. The milled suspensions were dried in an oven and ground in an alumina mortar. Samples denoted as "dry pressed" were uniaxially pressed in a 4 mm die at 20 MPa followed by cold isostatic pressing (CIP) at 200 MPa. Samples denoted as "tape cast" were tape cast according to the process detailed elsewhere.[16] Organics were removed by heating at 0.2°C/min to 600°C and held 12 h in air. After burnout, samples were CIPed at 200 MPa.

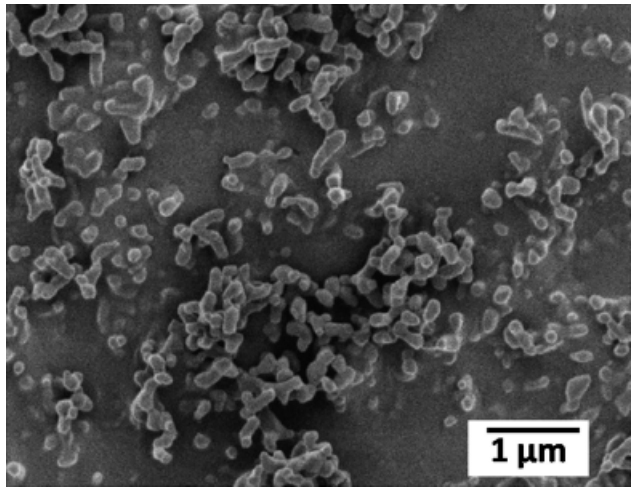

Fig. 1. FESEM micrograph of 1 at.% Nd:YAG powder used in this study calcined at 1150°C for 2 h and 1250°C for 10 h.

(2) Sintering

Samples were sintered in a pure YAG embedding powder that had been calcined in air at 1600°C for 40 h. The embedding powder contained no SiO_2. Sintering occurred between 1484° and 1750°C for up to 60 h in a tungsten mesh heated vacuum furnace (M60, Centorr Vacuum Industries, Nashua, NH) under 5×10^{-3} Torr. The heating and cooling rates were 10° and 20°C/min, respectively.

(3) Microstructural and Optical Characterization

Sintered density up to 99.9% was measured using the Archimedes method. Sintered densities over 99.9% were obtained by image analysis. For SEM imaging (XL20, Philips, Eindhoven, the Netherlands), the samples were ground with a diamond wheel and then polished sequentially on silk pads with 6, 1, and 0.25 μm diamond slurries. Sample thicknesses after polishing were nominally 1 mm. The polished specimens were thermally etched between 1300° and 1550°C for 0.25–10 h. Grain sizes and pore sizes of the sintered samples were obtained by the linear intercept method (at least 200 counts) where the average intercept length was multiplied by 1.56 to calculate the average grain size. In-line optical transmission on sintered samples annealed in air for 10 h at 1600°C was measured with a spectrophotometer with integrating sphere (Lambda 950, Perkin-Elmer, Wellesley, MA).

(4) Nuclear Magnetic Resonance (NMR)

NMR was used to determine the coordination and bonding environment of Si^{4+} in sintered Nd:YAG ceramics. Coprecipitated Nd:YAG powders were mixed with 0.14 wt% and 0.28 wt% ^{29}Si-enriched SiO_2 (SiO_2, 96.74% ^{29}Si, Cambridge Isotobe Laboratories, Andover, MA). Samples were milled, dry pressed, CIPed, and sintered at 1600°C for 2 h according to the procedure described above. The Nd:YAG samples were probed using ^{29}Si magic angle spinning (MAS) NMR. These experiments were carried out in a 7.0 T magnetic field with a Tecmag Discovery NMR spectrometer (Tecmag Inc., Houston, TX) operating at a ^{29}Si irradiation/detection frequency of 59.081 MHz. The spectrometer was interfaced to a 7.5 mm double resonance NMR probe that was run with MAS rates of 3 kHz. A spectral width of 40 kHz was covered with the acquisition of 2048 complex data points. For each spectrum, a total of 4220 scans was

acquired. The pulse length for irradiation of ^{29}Si was 7 μs, providing approximately 90° of spin nutation, and the recycle delay between pulses was 60 s.

(5) TEM

To observe grain-boundary structure and the spatial distributions of Nd^{3+} and Si in the microstructure, HRTEM was performed on tape cast Nd:YAG ceramics doped with 0.14 and 0.28 wt% SiO_2 sintered at 1700° and 1750°C for 8 h. A JEOL EM-2010F Field-Emission TEM/STEM (JEOL Ltd., Tokyo, Japan) equipped with an energy-dispersive X-ray spectroscopy (EDS) detector (Oxford Instruments, Abingdon, U.K.) and Gatan Enfina electron energy loss spectrometer (EELS) (Gatan Inc., Pleasanton, CA) was used for TEM characterization. The samples were polished to 0.5 μm surface roughness using diamond impregnated polymer films followed by argon ion milling on a liquid nitrogen cooling stage. HRTEM phase contrast images were taken along the [111] direction for one of two adjacent grains with the other grain showing clear lattice fringes.

III. Results and Discussion

(1) SiO_2 in Nd:YAG Ceramics

In this section, we investigate the coordination and distribution of Si^{4+} in ≤0.28 wt% SiO_2-doped Nd:YAG ceramics between 1600° and 1750°C to inform our discussions about the effects of SiO_2 on sintering and microstructure evolution.

Figure 2 shows the NMR spectrum obtained from 0.28 wt% SiO_2-doped Nd:YAG sintered at 1600°C for 2 h. Two overlapping peaks with full-width at half-maxima (FWHM) of 5 and 3 ppm are observed. A FWHM of 3–5 ppm is consistent with crystalline order (amorphous phases frequently have FWHM > 20 ppm), indicating that SiO_2 is primarily coordinated in highly crystalline environments. The −80 to −85 ppm chemical shift is consistent with tetrahedrally coordinated Si^{4+}.[21] Octahedrally coordinated Si^{4+} results in chemical shifts between −180 and −220 ppm, but no peaks were observed in this range. It is therefore clear that the majority of Si^{4+} occupies the tetrahedrally coordinated Al^{3+} 24(*d*) site as opposed to octahedrally coordinated Al^{3+} 16(*a*) sites in the YAG structure. This result confirms predictions from atomistic modeling that Si^{4+} preferentially occupies tetrahedral sites in YAG.

The two distinct $^{29}Si^{4+}$ peaks observed in Fig. 2 may be explained by cationic substitutions in the second coordination shell of the $^{29}Si^{4+}$. Fyfe *et al.*[21] observed similar chemical shifts in tetrahedrally coordinated $^{29}Si^{4+}$ when ionic substitutions occurred in the second coordination shell surrounding the $^{29}Si^{4+}$ tetrahedra. The second coordination shell of each Al^{3+} 24(*d*) site in YAG consists of eight Y^{3+} 24(*c*) sites and four octahedrally coordinated Al^{3+} 16(*a*) sites. In Nd:YAG, second coordination shell substitutions could occur by Nd^{3+} occupying a 24(*c*) site, or by antisite defects (Y^{3+} occupying 16(*a*) and 24(*d*) sites or Al^{3+} occupying 24(*c*) sites) which are known to occur in YAG ceramics and single crystals.[20,22]

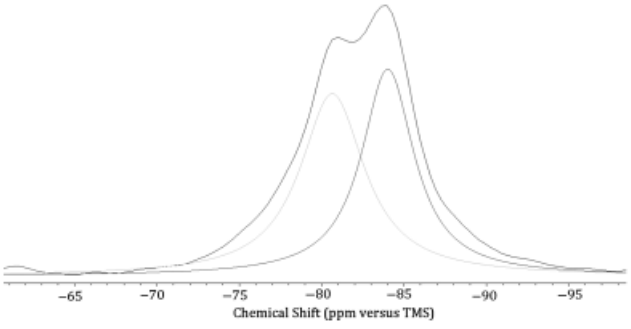

Fig. 2. NMR spectrum of dry pressed Nd:YAG doped with 0.28 wt% Si^{29}-enriched SiO_2 sintered at 1600°C for 2 h.

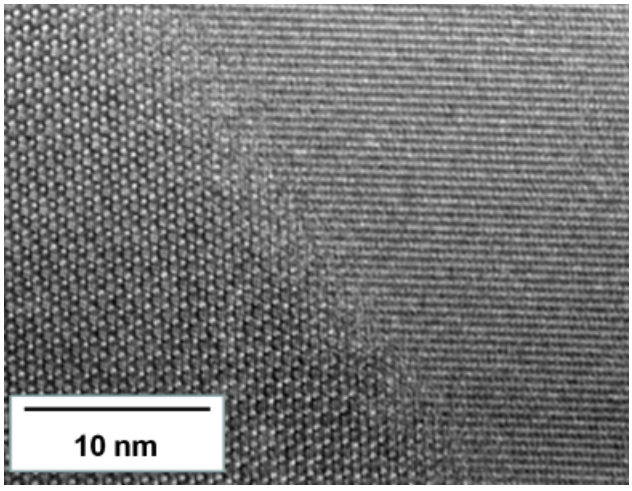

Fig. 3. HRTEM image of a grain boundary in tape cast 0.28 wt% SiO_2-doped Nd:YAG sintered at 1700°C for 8 h. No amorphous phase is observed at the grain boundary.

Figure 3 is an HRTEM micrograph of a grain boundary in 0.28 wt% SiO_2-doped Nd:YAG sintered at 1700°C for 8 h. The grain boundary is <1 nm thick with lattice fringes extending to the boundary of each grain. Grain boundaries and triple lines show no signs of crystalline second phases or amorphous phases in this sample or any other sample in this study. EELS was also used to detect Si. The k ionization edge for Si at 1839 eV was detected at grain centers, grain boundaries, and triple lines indicating that Si^{4+} substitutes into the YAG lattice and is also present at grain boundaries and triple points. This observation provides further evidence that Si^{4+} enters into a solid solution with the Nd:YAG lattice during sintering.

0.28 wt% SiO_2 doping corresponds to 0.5% of the available Al^{3+} sites in the YAG structure. Because SiO_2 was added to stoichiometric Nd:YAG powder, 0.28 wt% SiO_2 doping leads to 0.5 at.% Al^{3+} cation excess over the stoichiometric composition. The precise limit of stoichiometric variation in YAG ceramics is not known, but Patel *et al.*[22] found that Al^{3+} excess may be limited to 0.2 at.% by comparing lattice constant measurements from X-ray data with atomistic simulations of defect mechanisms. However, no evidence of second phases was found up to 0.62 at.% excess Al^{3+} in that study. Further, the YAG ceramics in Patel and colleagues were doped with 0.14 wt% SiO_2, but Si^{4+} content was not considered when determining sample stoichiometry. After accounting for Si^{4+} in the sample stoichiometry, the Al^{3+} excess limit in SiO_2-doped YAG ceramics is at least 0.45 at.%. Clearly, further work is required to determine the precise limits of nonstoichiometry in SiO_2-doped YAG ceramics. In the present study, no second phases were observed by SEM or TEM in any sample, thus it is likely that Al^{3+} excess caused by Si^{4+} doping does not result in second phase formation up to at least 0.28 wt% SiO_2.

Given that the chemical shift and relatively narrow FWHM observed in Fig. 2, the fact that Si is detected at grain interiors by EELS, and that grain boundaries observed by HRTEM (Fig. 3) show no evidence of an amorphous phase, we conclude that Si^{4+} primarily exists as solute ions located at tetrahedrally coordinated 24(*d*) sites in the YAG crystal structure for ≤0.28 wt% SiO_2-doped Nd:YAG ceramics sintered between 1600° and 1750°C.

(2) Densification

Figure 4 shows relative density during final stage densification as a function of temperature and time for tape cast Nd:YAG ceramics doped with 0.035–0.28 wt% SiO_2. Increasing silica content increases density at all temperatures and times. The 0.28 wt% SiO_2-doped samples densify to over 99.9% relative

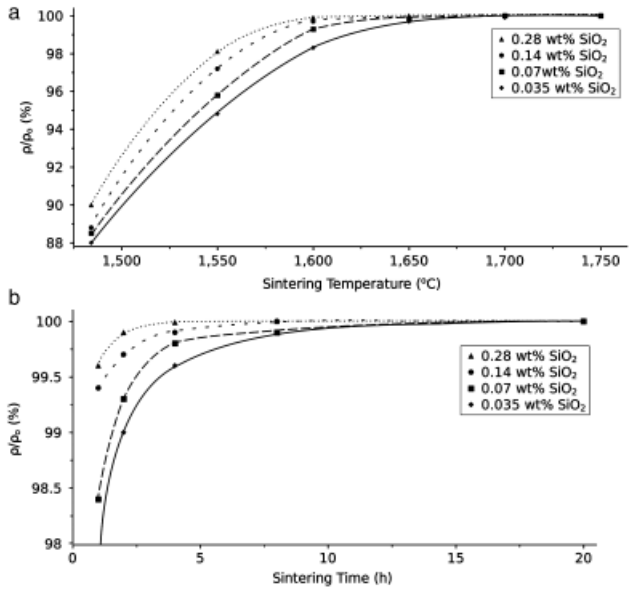

Fig. 4. (a) Relative density versus temperature for tape cast Nd:YAG samples doped with 0.035, 0.07 0.14, and 0.28 wt% SiO_2. Holding time was 2 h. (b) Relative density versus sintering time at 1600°C for tape cast Nd:YAG samples doped with 0.035, 0.07, 0.14, and 0.28 wt% SiO_2.

density at short times (2 h for all temperatures >1600°C) and low temperatures (1600°C for 8 h) while samples doped with less SiO_2 achieve $>99.9\%$ density at longer times (8–20 h) and/or higher temperatures (1750°C). Figure 4(b) shows that all samples sinter to over 99.9% density after 20 h at 1600°C. While all samples had measured densities over 99.9% after sintering at 1600°C for 20 h, only the 0.28 wt% SiO_2-doped Nd:YAG samples were highly transparent ($>80\%$ in-line transmission at 1064 nm) at this sintering condition.

To explain the increasing densification rate as a result of increasing SiO_2 content, we examine the effect of Si^{4+} substitution on Y^{3+} and Nd^{3+} diffusion. Y^{3+} and rare earth ion (Nd^{3+}, Er^{3+}, Yb^{3+}, etc.) diffusion is reported to be the rate limiting factor for both grain boundary and lattice diffusion in YAG ceramics.[23,24] This implies that increasing Y^{3+} and Nd^{3+} diffusion rates should also lead to faster densification kinetics. Ionic diffusion in ceramics typically occurs by a vacancy mechanism and the self diffusion coefficient can be written[25]:

$$D = D_0 \exp\left[\frac{-E_j}{k_B T}\right] \tag{2}$$

where D is the diffusion constant, E_j is the activation energy to jump to an adjacent vacancy, k_B is Boltzmann's constant, T is temperature, and D_0 is[25]:

$$D_0 = fa^2 v X_v \tag{3}$$

where f is the correlation factor, a is the nearest neighbor jump distance, v is the jump frequency, and X_v is the site fraction of vacancies on the appropriate sublattice. According to Eq. (1), X_v should increase on the Y^{3+}/Nd^{3+} sublattice with increasing SiO_2 content. According to Eqs. (2) and (3), increasing X_v will in turn cause both $D_{Y^{3+}}$ and $D_{Nd^{3+}}$ to increase with increasing SiO_2 content. Diffusion experiments on Nd_2O_3 coated YAG ceramics confirm that Nd^{3+} lattice and grain-boundary diffusion constants increase with increasing silica content.[24] Thus, by creating vacancies on the Y^{3+}/Nd^{3+} sublattice (Eq. 1), and thereby increasing diffusion rates for both Y^{3+} and Nd^{3+}, SiO_2 doping increases densification kinetics in Nd:YAG ceramics.

Figure 5 shows representative microstructures of 0.035 wt% SiO_2-doped Nd:YAG sintered for 2 h (Fig. 5a), 4 h (Fig. 5b), and 20 h (Figs. 5c and d) at 1600°C. The isolated pores in the images are typical of final stage densification in SiO_2-doped Nd:YAG ceramics. Pores are similar in size to grains and are separated by large defect-free regions, i.e., regions where there are no pores or second phases present at grain boundaries and triple points. In samples with densities $>99.9\%$, these defect-free regions (shown in Fig. 5(d)) were observed to be $>900\ \mu m^2$. In order to sinter to the exceptionally high densities ($>99.995\%$) required for high efficiency laser materials, we must consider final stage sintering characterized by a small number of pores, similar in size to the average grain size, separated

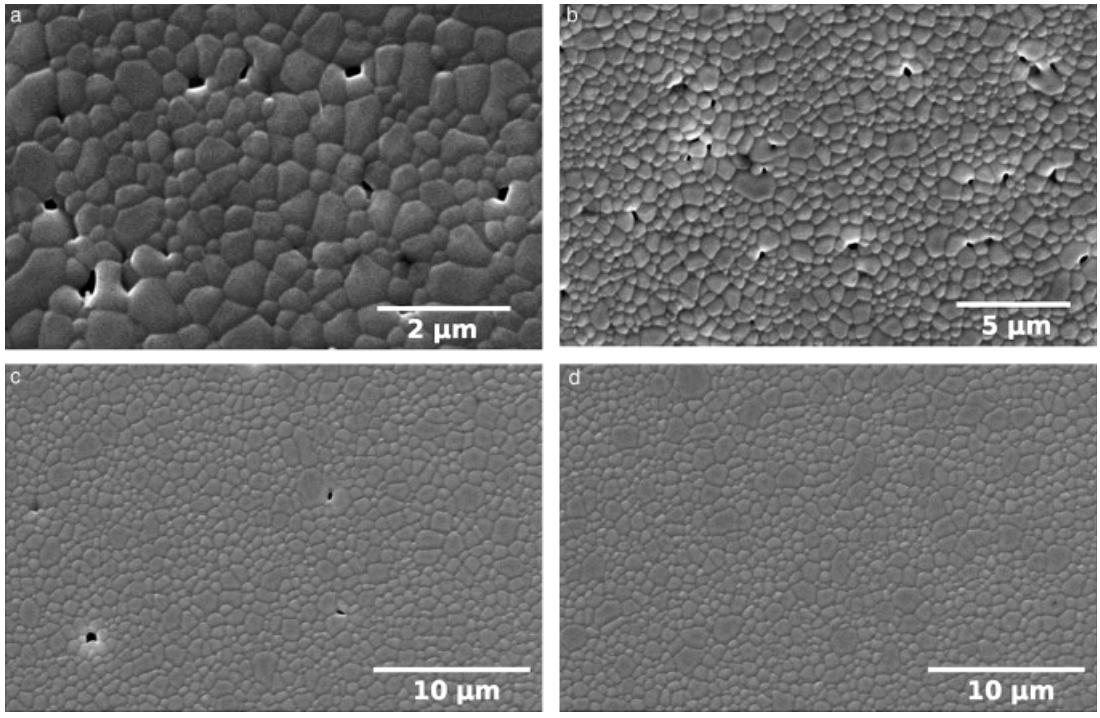

Fig. 5. SEM micrographs of tape cast Nd:YAG ceramics doped with 0.035 wt% SiO_2 sintered at 1600°C for 2 h (a) and 8 h (b) and 20 h (c and d).

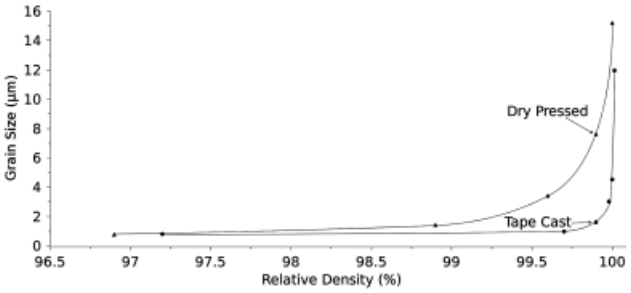

Fig. 6. Sintering trajectory for tape cast and dry pressed 0.14 wt% SiO_2-doped Nd:YAG ceramics sintered between 1550°C and 1750°C for 2–8 h.

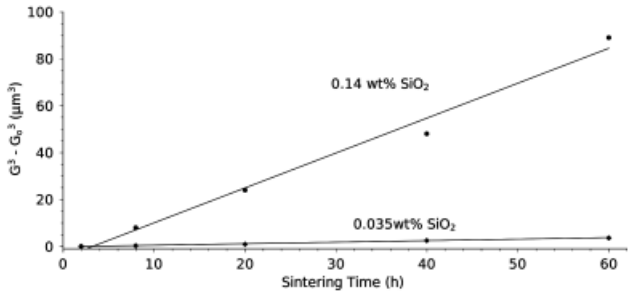

Fig. 8. G^3–G_0^3 vs sintering time at 1600°C for tape cast Nd:YAG ceramics containing 0.035, and 0.14wt% SiO_2.

by multigrain distances, rather than small pores distributed along grain boundaries and triple lines.

Because of large pores like those observed in Fig. 5 usually result from green forming defects, we investigated the role of green forming on microstructural development and densification. Dry pressed and tape cast samples doped with 0.14 wt% SiO_2 were sintered between 1484° and 1750°C for 1–8 h. The average green densities of tape cast and dry pressed samples were 48.3% and 44.7%, respectively, and the sample thicknesses after sintering were 2 mm for both tape cast and dry pressed samples.

Figure 6 shows that tape cast samples have smaller average grain size at the same density as dry pressed samples. Because dry pressed samples have a small population of larger pores that are not found in tape cast samples,[16] dry pressed materials require longer sintering times and higher sintering temperatures to achieve comparable densities to tape cast samples. The longer sintering times and higher sintering temperatures required in dry pressed samples lead to larger average grain sizes at identical sintered densities compared with tape cast samples. Clearly, the sintering trajectory is affected by the green forming process, and as demonstrated in Fig. 6, colloidal methods like tape casting are better suited than dry pressing to achieving fine-grained transparent ceramics by pressureless densification. This data coincides well with previous studies[26] that found that colloidal processing methods lead to increased particle packing homogeneity and, therefore, decreased sintering temperatures than dry pressing. Also, because all samples in this study sintered to >99.9% density at 1600°C and densification was only limited by a small number of large pores, refining green forming procedures to increase green density and particle packing homogeneity would eliminate these large pores thus enabling sintering of transparent Nd:YAG in low silica content (i.e., <0.14 wt%) ceramics at 1600°C.

(3) Grain Growth

Figure 7 shows the effects of temperature on grain growth for 0.035–0.28 wt% SiO_2-doped Nd:YAG. Increasing silica content increases grain size under all conditions. The 0.035 wt% silica content samples maintain grain sizes below 3 μm even at sintering conditions up to 1750°C for 8 h. To determine the grain growth exponent (n) and rate constant (k), kinetic data was plotted according to the following equation:

$$G^n - G_0^n = kt \tag{4}$$

where G is the average grain size, G_0 is taken to be the grain size at 2-h hold time for each temperature, and t is time. Grain growth data was fit to n values of 2–4. $n = 3$ provided the best fit for all temperatures and compositions (linear regression R^2 parameters ranged from 0.93 to 0.99). Boulesteix *et al.*[11] and Kochawattana *et al.*[24] also found that grain growth kinetics fit a cubic rate law for temperatures between 1525° and 1850°C. Figure 8 shows grain growth kinetics for tape cast 0.035 and 0.14 wt% SiO_2-doped Nd:YAG sintered at 1600°C for 2–60 h plotted according to Eq. (4) with $n = 3$.

As shown in Fig. 5, the vast majority of grain boundaries do not intersect pores. Therefore, it is likely that grain growth for samples sintered at >1600°C is controlled by grain-boundary mobility rather than pore drag. In boundary-controlled systems, grain growth exponents equal to 3 are explained by either diffusion-controlled growth in liquid phase containing systems or by solute drag mechanisms in solid-state systems.[27] As shown above, no liquid phase is observed in <0.28 wt% SiO_2-doped Nd:YAG ceramics sintered between 1600° and 1750°C, and thus we conclude that the cubic grain growth kinetics observed in Fig. 8 are due to solute drag.

As noted above, Y^{3+} and rare-earth ion diffusion limit mass transport in YAG ceramics. Because Nd^{3+} has both a larger ionic radius and a greater atomic mass than Y^{3+}, it is expected to have a slower diffusion rate than Y^{3+}. Therefore, the ion in Nd:YAG most likely to result in solute drag during grain growth is Nd^{3+}.

During solute drag limited grain growth, the concentration of the slow-diffusing solute atoms is higher at or near grain boundaries than the grain interiors. Therefore, if Nd^{3+} causes solute drag in the Nd:YAG system, we should find higher Nd^{3+} concentrations near grain boundaries. Figure 9 shows the Gibbsian interfacial excess (γ) of Nd^{3+} at grain boundaries as determined by TEM EDS analysis of relative Nd^{3+} content

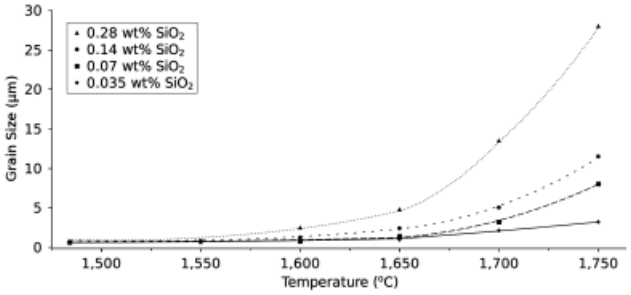

Fig. 7. Grain size as a function of temperature between 1484°C and 1750°C for tape cast Nd:YAG ceramics doped with 0.035, 0.07, 0.14, and 0.28 wt% SiO_2. Sintering time was 2 h at each temperature.

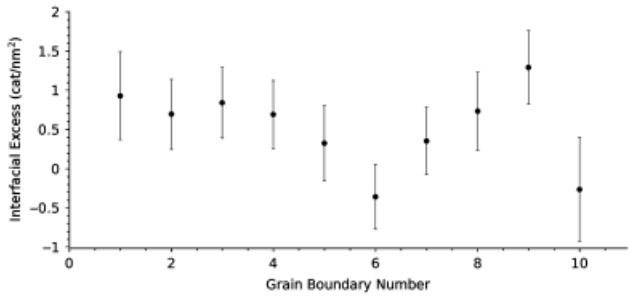

Fig. 9. Interfacial excess of Nd^{3+} at grain boundaries in 0.14 wt% SiO_2-doped Nd:YAG sintered at 1700°C for 8 h.

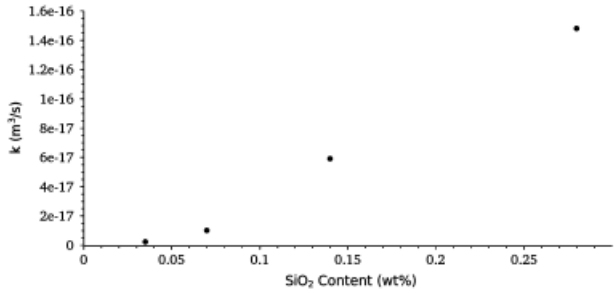

Fig. 10. Grain growth rate constant, k, versus SiO_2 content for tape cast Nd:YAG ceramics doped with 0.035, 0.07, 0.14, and 0.28 wt% SiO_2 sintered at 1700°C for 2–8 h.

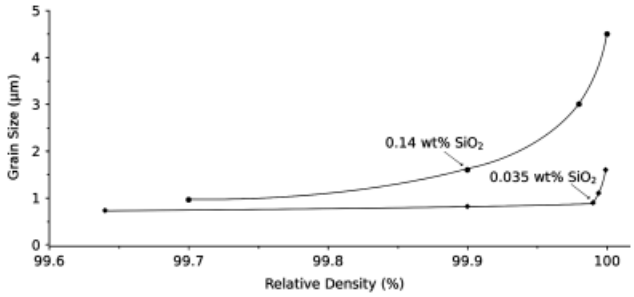

Fig. 12. Sintering trajectory for tape cast Nd:YAG ceramics containing 0.035 and 0.14 wt% SiO_2 sintered at 1600°C for 8–60 h.

between grain boundaries and grain interiors where Γ is calculated according to the following equation[28]:

$$\Gamma = N_Y \left[\left(\frac{C_{Nd}}{C_Y} \right)^{GB} - \left(\frac{C_{Nd}}{C_Y} \right)^{GI} \right] w \quad (5)$$

where N_Y is the number density of Y^{3+} lattice sites, C_{Nd} is Nd^{3+} concentration, C_Y is Y^{3+} concentration, w is the width of the analysis area (33 nm) and GB and GI refer to measurements taken at the grain boundary and grain interior, respectively. The average interfacial excess for 10 boundaries was 0.789 Nd^{3+} nm^{-2}. This correlates to an absolute concentration of 1.25 at.% Nd^{3+} at grain boundaries which is 25% more than the as-batched composition. Optical techniques have also shown Nd^{3+} segregation at grain boundaries. Ramirez *et al.*[29] used confocal scanning optical microscopy (CSOM) and also showed that Nd^{3+} concentration increased at grain boundaries by 10% relative to grain interiors in 0.14 wt% SiO_2-doped Nd:YAG. The lower spatial resolution of CSOM (<0.5 μm × 0.5 μm × 2–3 μm) relative to TEM may account for the differences in grain-boundary concentration observed by the two techniques. A similar analysis was not performed for Si^{4+} because the Y L_α peak overlaps with the Si$K\alpha$ peak.

Grain growth constants (k) were calculated according to Eq. (4) for 0.035, 0.07, 0.14, and 0.28 wt% SiO_2-doped Nd:YAG samples sintered at 1600°, 1650°, 1700°, and 1750°C for 2–8 h.

Figures 10 and 11 show that k increases as a function of SiO_2 doping for samples sintered for 2–8 h at 1700°C and all sintering temperatures used in this study. Cahn[30] showed that boundary mobility (M_b) in a solute drag limited system should vary with grain-boundary diffusivity of the solute atoms (D_b) according to the following eqaution[30]:

$$M_b = \frac{\Omega}{k_B T \delta_{gb}} \left(\frac{1}{D_a} + \frac{4 N_V \Omega Q C_\infty}{D_b} \right)^{-1} \quad (6)$$

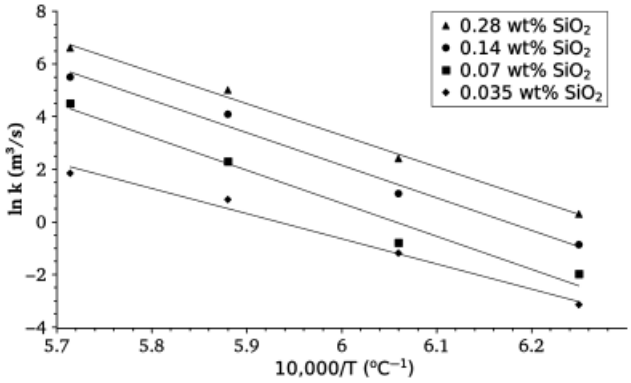

Fig. 11. Arrhenius plot of ln k vs $1/T$ for tape cast 0.035, 0.07, 0.14 and 0.28 wt% SiO_2-doped Nd:YAG sintered between 1600° and 1750°C for 2–8 h.

where ω is molar volume, δ_{gb} is the grain-boundary thickness, D_a is the diffusivity of the solvent ions, N_v is the solvent atom concentration, Q is the partition coefficient, and C_∞ is the solute atom concentration in the grain center. As shown above, increasing SiO_2 content increases both Y^{3+} and Nd^{3+} diffusivity in YAG which increases both D_a and D_b in Eq. (6). Because increasing M_b increases k as well, this analysis provides a plausible explanation that is consistent with a solute drag hypothesis for the increasing grain growth rate as a function of SiO_2 content.

The activation energy for grain growth between 1600° and 1750°C was calculated using the Arrhenius equation:

$$\ln(k) = \frac{-E_a}{k_B T} + C \quad (7)$$

where k is the rate constant in Eq. (4), E_a is the activation energy, and C is a constant. Figure 11 shows the Arrhenius plots for each silica content. The calculated activation energies for grain growth of 0.035-, 0.07-, 0.14-, and 0.28 wt% SiO_2-doped samples were 960, 1210, 1130, and 1160 kJ/mol, respectively. These values are consistent with the activation energy for grain growth in SSR ceramics sintered between 1700° and 1850°C by Kochawattana *et al.*[11]

(4) Microstructural Control and Sintering Trajectory

Along with green forming, understanding the links between sintering temperature, silica content, densification rate, and grain growth rate is key to controlling microstructure evolution in transparent Nd:YAG. Figure 12 shows grain size as a function of density for tape cast 0.035 and 0.14 wt% SiO_2-doped Nd:YAG sintered at 1600°C for 8–60 h. Figures 4 and 7 show that increasing SiO_2 content increases both densification and coarsening, and Fig. 12 shows that the sintering trajectory begins to follow a more coarsening path in samples with increasing SiO_2 content. While increasing SiO_2 content leads to higher

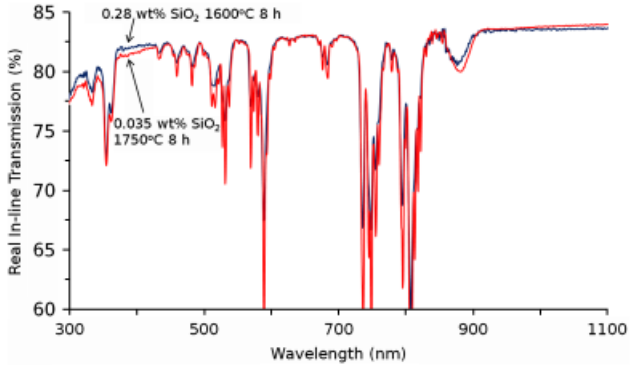

Fig. 13. In-line transmission for tape cast 0.0.35 wt% SiO_2 Nd:YAG sintered at 1750°C for 8 h and 0.28 wt% SiO_2 Nd:YAG sintered at 1600°C for 8 h. Grain sizes were 2.8 and 18 μm and sample thicknesses were 1.3 and 1.1 mm, respectively.

densities at lower sintering temperatures and shorter times, comparable densities in samples with lower SiO_2 content have smaller average grain size.

Figure 13 shows the in-line transmission for tape cast Nd:YAG samples doped with 0.035 and 0.28 wt% SiO_2. The polished samples were 1.3 and 1.1 mm thick, respectively. At 0.28 wt% silica content, highly transparent ceramics with an 18 μm average grain size were achieved by sintering at 1600°C for 8 h. In the case of 0.035 wt% SiO_2, highly transparent ceramics with 2.8 μm average grain size were achieved after sintering at 1750°C for 8 h. These samples clearly illustrate the relationships between SiO_2 content, sintering kinetics, and sintering trajectory. The faster densification kinetics in the 0.28 wt% SiO_2-doped sample lead to transparency at a relatively low temperature (1600°C), but the more coarsening sintering trajectory leads to a relatively large average grain size (18 μm). Lower SiO_2 content in 0.035 wt% SiO_2 samples leads to slower densification kinetics requiring higher sintering temperatures and longer times to achieve transparency. However, the more densifying sintering trajectory in 0.035 wt% SiO_2-doped samples leads to finer grained transparent materials despite the higher temperatures required to sinter to transparency.

A possible explanation for the more coarsening sintering trajectory observed in samples with higher SiO_2 contents centers on the relative effects of Si^{4+} doping on grain-boundary (D_{gb}) and lattice diffusion (D_l). Boulesteix *et al.*[24] showed the Nd^{3+} grain-boundary diffusion increased by up to two times more than volume diffusion between 0 and 0.3 wt% SiO_2-doped Nd:YAG ceramics. To understand why increasing grain-boundary diffusion should increase coarsening at a greater rate than densification, we consider common models for densification and grain growth. Herring showed that densification rate can be described by the following equation[31]:

$$\frac{d\rho}{dt} = F(\rho)\left(\frac{3\pi\Omega\gamma}{k_B T}\right)\left\{\frac{D_{gb}\delta_b}{G^4} + \frac{D_l}{G^3}\right\} \quad (8)$$

where D_{gb} is the grain-boundary diffusion coefficient and $F(\rho)$ is a microstructurally dependent function of density. Cahn[30] showed that grain growth rate in solute drag limited systems is inversely proportional to G^2 according to the following equation[30]:

$$\frac{dG}{dt} \propto \left\{\frac{D_{gb}}{G^2}\right\} \quad (9)$$

(Because Eq. [9] is grain growth rate, it is the partial first derivative with respect to time of Eq. [4] and is thus consistent with the cubic rate law determined using Eq. [4].) Equations (8) and (9) show that for the same grain size, increasing D_{gb} increases grain growth rate faster than densification rate. For example, assuming a 2 μm average grain size and a 10% increase in D_{gb}, densification rate increases by 0.63% while the grain growth rate increases by 2.5%. Therefore, increased SiO_2 doping in Nd:YAG ceramics leads to a more coarsening sintering trajectory by preferentially increasing D_{gb} over D_l, and increasing dG/dt faster than $d\rho/dt$.

IV. Conclusions

Both densification and grain growth in Nd:YAG increase with increasing SiO_2 content. SiO_2 contents up to 0.28 wt% doping form a complete solid solution with Nd:YAG at temperatures between 1600° and 1750°C, as evidenced by clean grain boundaries, the detection of Si at grain interiors, and narrow NMR peaks. TEM EDS analysis showed that Nd^{3+} concentration is higher at grain boundaries than the grain interiors by 25%. Nd^{3+} grain-boundary segregation and cubic grain growth kinetics indicate that coarsening in Nd:YAG ceramics is controlled by a solute drag mechanism. Because densification is limited by small numbers of large pores, colloidal processing leads to lower sintering times and temperatures as well as decreased grain size at the same density as dry pressed samples. As silica content increases, the sintering trajectory in Nd:YAG ceramics occurs along an increasingly coarsening path. Higher silica content samples densify at lower temperatures and times than lower silica content samples. Lower silica content samples may achieve full density by sintering at relatively high temperatures, but the more densifying sintering trajectory leads to smaller average grain sizes than higher silica content samples sintered at lower temperatures.

References

[1]R. L. Coble, "Transparent Alumina and Method of Preparation"; U.S. Patent 3026210, March 20, 1962.

[2]G. J. Peelen and R. Metselaar, "Light-Scattering by Pores in Polycrystalline Materials—Transmission Properties of Alumina," *J. Appl. Phys.*, **45** [1] 216–20 (1974).

[3]R. D. Anderson, "Transparent Yttria-Based Ceramics and Method for Producing Same"; U.S. Patent No. 3545987, December 8, 1970.

[4]D. W. Roy and F. J. Stermole, "Method for Manufacturing a Transparent Ceramic Body"; U.S. Patent 3974249, August 10, 1976.

[5]W. McCauley and N. D. Corbin, "Phase Relations and Reaction Sintering of Transparent Cubic Aluminum Oxynitride Spinel (ALON)," *J. Am. Ceram. Soc.*, **62** [9–10] 476–9 (1979).

[6]A. Ikesue, I. Furusato, and K. Kamata, "Fabrication Of Polycrystalline, Transparent YAG Ceramics By A Solid-State Reaction Method," *J. Am. Ceram. Soc.*, **78** [1] 225–8 (1995).

[7]Y. Aung and A. Ikesue, "Ceramic Laser Materials," *Nat. Photon.*, **2** [12] 721–7 (2008).

[8]J. R. Lu, M. Prabhu, J. Q. Xu, K. Ueda, H. Yagi, T. Yanagitani, and A.A Kaminskii, "Highly Efficient 2% Nd:Yttrium Aluminum Garnet Ceramic Laser," *Appl. Phys. Lett.*, **77** [23] 3707–9 (2000).

[9]J. Lu, K. Takaichi, T. Uematsu, A. Shirakawa, M. Musha, J.F Bisson, K. Ueda, H. Yagi, T. Yanagitani, and A.A Kaminskii, "Nd^3:$YGdO_3$ Ceramic Laser," *Laser Phys.*, **13** [7] 940–2 (2003).

[10]S.-H. Lee, S. Kochawattana, G. L. Messing, J. Q. Dumm, G. Quarles, and V. Castillo, "Solid-State Reactive Sintering of Transparent Polycrystalline Nd:YAG Ceramics," *J. Am. Cer. Soc.*, **89** [6] 1945–50 (2006).

[11]S. Kochawattana, A. J. Stevenson, S.-H. Lee, M. Ramirez, V. Gopalan, J. Dumm, V. K. Castillo, G. J. Quarles, and G. L. Messing, "Sintering and Grain Growth in SiO_2 Doped Nd:YAG," *J. Eur. Ceram. Soc.*, **28** [7] 1527–34 (2008).

[12]J. R. Lu, T. Murai, K. Takaichi, T. Uematsu, K. Misawa, M. Prabhu, J. Xu, K. Ueda, H. Yagi, T. Yanagitani, A.A Kaminskii, and A. Kudryashov, "72 W Nd:$Y_3Al_5O_{12}$ Ceramic Laser," *Appl. Phys. Lett.*, **78** [23] 3586–8 (2001).

[13]J. Lu, H. Yagi, K. Takaichi, T. Uematsu, J.-F. Bisson, Y. Feng, A. Shirakawa, K.-I. Ueda, T. Yanagitani, and A. A. Kaminskii, "110 W Ceramic Nd_3:$Y_3Al_5O_{12}$ Laser," *App. Phys. B*, **79** [1] 25–8 (2004).

[14]K. Otsuka, T. Narita, Y. Miyasaka, C.-C. Lin, J.-Y. Ko, and S.-C. Chu, "Nonlinear Dynamics in Thin-Slice Nd:YAG Ceramic Lasers: Coupled Local-Mode Laser Model," *Appl. Phys. Lett.*, **89** [8] 081117–3 (2006).

[15]J. R. Lu, K. Ueda, H. Yagi, T. Yanagitani, Y. Akiyama, and A.A Kaminskii, "Neodymium Doped Yttrium Aluminum Garnet ($Y_3Al_5O_{12}$) Nanocrystalline Ceramics—A New Generation of Solid State Laser and Optical Materials," *J. Alloys Compd.*, **341** [1–2] 220–5 (2002).

[16]S.-H. Lee, E. R. Kupp, A. J. Stevenson, J. M. Anderson, G. L. Messing, X. Li, E. C. Dickey, J. Q. Dumm, V. K. Simonaitis-Castillo, and G. J. Quarles, "Hot Isostatic Pressing of Transparent Nd:YAG Ceramics," *J. Am. Ceram. Soc.*, **92** [7] 1456–63 (2009).

[17]O. Fabrichnaya, H. J. Seifert, R. Weiland, T. Ludwig, F. Aldinger, and A. Navrotsky, "Phase Equilibria and Thermodynamics in the Y_2O_3–Al_2O_3–SiO_2 System," *Z. Metall.*, **92** [9] 1083–97 (2001).

[18]R. Boulesteix, A. Maître, J.-F. Baumard, C. Sallé, and Y. Rabinovitch, "Mechanism of the Liquid-Phase Sintering for Nd:YAG Ceramics," *Opt. Mater.*, **31** [5] 711–5 (2009).

[19]A. Ikesue, K. Yoshida, T. Yamamoto, and I. Yamaga, "Optical Scattering Centers in Polycrystalline Nd:YAG Laser," *J. Am. Ceram. Soc.*, **80** [6] 1517–22 (1997).

[20]M. M. Kuklja, "Defects in Yttrium Aluminium Perovskite and Garnet Crystals: Atomistic Study," *J. Phys.: Condens. Mater.*, **12** [13] 2953–67 (2000).

[21]C. A. Fyfe, Y. Feng, H. Grondey, G. T. Kokotailo, and H. Gies, "One- and Two-Dimensional High-Resolution Solid-State NMR Studies of Zeolite Lattice Structures," *Chem. Rev.*, **91** [7] 1525–43 (1991).

[22]A. P. Patel, M. R. Levy, R. W. Grimes, R. M. Gaume, R. S. Feigelson, K. J. McClellan, and C. R. Stanek, "Mechanisms of Nonstoichiometry in $Y_3Al_5O_{12}$," *Appl. Phys. Lett.*, **93** [19] 191902–4 (2008).

[23]M. Jiménez-Melendo, H. Haneda, and H. Nozawa, "Ytterbium Cation Diffusion in Yttrium Aluminum Garnet (YAG): Implications for Creep Mechanisms," *J. Am. Ceram. Soc.*, **84** [10] 2356–60 (2001).

[24]R. Boulesteix, A. Maître, J.-F. Baumard, Y. Rabinovitch, C. Sallé, S. Weber, and M. Kilo, "The Effect of Silica Doping on Neodymium Diffusion in Yttrium Aluminum Garnet Ceramics: Implications for Sintering Mechanisms," *J. Eur. Ceram. Soc.*, **29** [12] 2517–26 (2009).

[25]R. W. Baluffi, S. M. Allen, and W. C. Carter, *Kinetics of Materials*. Wiley-Interscience, New York, 2005.

[26]A. Krell and J. Klimke, "Effects of the Homogeneity of Particle Coordination on Solid-State Sintering of Transparent Alumina," *J. Am. Ceram. Soc.*, **89** [6] 1985–92 (2006).
[27]R. J. Brook, "Ceramic Fabrication Processes"; pp 331–64, *Treatise on Materials Science and Technology*, Vol. 9, Edited by F. F. W. Wang. Academic, New York, 1976.
[28]J. Goldstein, D. C. Joy, and A. D. Romig Jr., *Principles of Analytic Electron Microscopy*. Springer, New York, 1986.
[29]M. O. Ramirez, J. Wisdom, H. Li, Y. L. Aung, J. Stitt, G. L. Messing, V. Dierolf, Z. Liu, A. Ikesue, R. L. Byer, and V. Gopalan, "Three-Dimensional Grain Boundary Spectroscopy in Transparent High Power Ceramic Laser Materials," *Opt. Exp.*, **16** [9] 5965–73 (2008).
[30]J. W. Cahn, "The Impurity-Drag Effect in Grain Boundary Motion," *Acta Metall.*, **10** [9] 789–98 (1962).
[31]C. Herring, "Effect of Change of Scale on Sintering Phenomena," *J. Appl. Phys.*, **21**, 301–3 (1950). □